mater.scichina.com link.springer.com

Published online 11 August 2020 | https://doi.org/10.1007/s40843-020-1384-9
Sci China Mater 2020, 63(11): 2325–2334

Enhanced energy storage properties and temperature stability of fatigue-free La-modified $PbZrO_3$ films under low electric fields

Xiaojun Qiao[1], Wenping Geng[1], Xi Chen[1], Le Zhang[1], Dongwan Zheng[1], Liaoyuan Zhang[1], Jian He[1], Xiaojuan Hou[1], Yun Yang[1], Min Cui[1], Kaiyang Zeng[2*] and Xiujian Chou[1*]

ABSTRACT **Electrostatic energy-storage capacitors, with their ultrahigh storage density and high temperature stability, have been receiving increasing attention of late for their ability to meet the critical requirements of pulsed power devices in low-consumption systems. In such a context, this work reports on the successful production of anti-ferroelectric (AFE) thin films with excellent energy storage performance under a relatively low electric field. In particular, La-doped $PbZrO_3$ thin films were fabricated using a sol-gel method, yielding a recoverable energy storage density of 34.87 J cm^{-3} with an efficiency of 59.23% at room temperature under the electric field of ~800 kV cm^{-1}. The temperature dependence of the energy storage property was demonstrated from room temperature to 210°C, indicating a stable density variation between 34.87 and 27.98 J cm^{-3}. The films also exhibited excellent anti-fatigue property (endurance of up to 3×10^9 cycles and the recoverable energy storage density varied from 39.78 to 29.32 J cm^{-3} combined with an efficiency of 61.03%–44.95% under the test frequencies from 10 to 5000 Hz). All results were obtained using compact films with a high polarization (P_{max}) of approximately 103.7 μC cm^{-2} and low remnant polarization (P_r~7 μC cm^{-2}), which was owing to the combination of $LaNiO_3$ buffer layers and vacancies at Pb sites. These results illustrate the great potential of pulsed power devices in low-consumption systems operating in a wide range of temperatures and long-term operations.**

Keywords: antiferroelectric, energy storage, sol-gel, $PbZrO_3$ thin film, stability

INTRODUCTION

Energy storage capacitors with excellent temperature stability have been receiving increasing attention for applications in low-consumption systems and high-frequency pulsed devices owing to their high permittivity, excellent energy storage properties and fast charge-discharge properties [1–5]. In particular, ferroelectric (FE), relaxor ferroelectric (RFE), and antiferroelectric (AFE) materials have been studied owing to their nonlinear responses under external electric fields [2,4]. However, owing to the large remnant polarization (P_r) of FE materials, most of the energy is dissipated during the depolarization process, limiting their applications in energy-storage capacitors [6–9]. AFE materials have been widely studied for energy storage applications because they can release a greater number of charges owing to the absence of any P_r. The energy storage density of ceramics is limited by the low breakdown strength (<100 kV cm^{-1}) which was owing to the presence of defects, hindering their applications for energy storage devices [10–13]. For example, the energy storage densities of 5.6 and 6.4 J cm^{-3} were obtained in $Pb_{0.97}La_{0.02}(Zr_{0.5}Sn_{0.45}Ti_{0.05})O_3$ and $(Pb_{0.858}Ba_{0.1}La_{0.02}Y_{0.008})(Zr_{0.65}Sn_{0.3}Ti_{0.05})$ ceramics, respectively [12,13]. Compared with bulk ceramics, dielectric film capacitors can be ideal choices for applications in energy storage devices [14–20].

Recently, $PbZrO_3$-based (PZO) AFE films such as (Pb,La)ZrO_3 [6,20], (Pb,La)(Zr,Ti)O_3 (PLZT) [7,9], (Pb,La)(Zr,Sn,Ti)O_3 [12], and $Pb_{0.8}Ba_{0.2}ZrO_3$ (PBZ) [15] have been considered as promising candidates for pulsed power devices owing to their high maximum polarization (P_{max}) combined with small P_r and the fact that FE states can be obtained from their initial AFE states under sufficient electric fields. However, the recovery storage

[1] Science and Technology on Electronic Test and Measurement Laboratory, School of Instrument and Electronics, North University of China, Taiyuan 030051, China
[2] Department of Mechanical Engineering, National University of Singapore, Singapore 117576, Singapore
* Corresponding authors (emails: mpezk@nus.edu.sg (Zeng K); chouxiujian@nuc.edu.cn (Chou X))

density reported is typically small under low-strength electric fields, which precludes low-consumption applications. For example, large energy storage density of 18.8 J cm^{-3} was observed in Eu-doped PZO films under electric field of ~900 kV cm^{-1}, and high energy storage density of 21 J cm^{-3} under a bias field of 1300 kV cm^{-1} was obtained in $Pb_{0.97}Y_{0.02}[(Zr_{0.6}Sn_{0.4})_{0.925}Ti_{0.075}]O_3$ thin films [16,17]. Previous reports revealed that the doping of La element leads to the formation of vacancies at Pb sites, which is beneficial for the improvement of domain kinetics and energy storage [9,12]. A large energy storage density of 38 J cm^{-3} was obtained in AFE $(Pb_{1-x}La_x)(Zr_{0.85}Ti_{0.15})O_3$ thick films [9], and high energy storage density of 14.9 J cm^{-3} was achieved in $Pb_{0.95}La_{0.05}ZrO_3$ (PLZO) films [20]. To obtain higher energy storage density, further studies have focused on the enhancement of breakdown strength through various fabrication techniques (Table 1). In addition, the temperature stability is also critical for energy storage devices. However, few studies have been conducted with the aim of achieving higher energy storage density under much lower electric fields. Thus, exploring the electric properties of La-doped PZO films under low electric fields and harsh conditions is indispensable for attaining applicability to low-consumption pulsed power devices.

EXPERIMENTAL SECTION

Material preparation

The La-doped $PbZrO_3$ heterostructure was fabricated using a sol-gel method. Lead acetate trihydrate and lanthanum acetate were dissolved in 2-methoxyethanol, with a 10% excess in Pb to compensate for loss during the thermal process and to avoid the formation of pyrochlore. Zirconium *n*-propoxide was added into the solution at room temperature, and ethylene glycol was also added to improve mechanical properties. Finally, the solution with a concentration of 0.4 mol L^{-1} was obtained by adding

Table 1 Comparison of the energy storage properties of selected materials

Composition	P_{max} (μC cm^{-2})	E_{AF} (kV cm^{-1})	E_{FE} (kV cm^{-1})	Method	E (kV cm^{-1})	W (J cm^{-3})	η (%)	Ref.
$(Pb_{0.965}La_{0.035})(Zr_{0.9}Ti_{0.1})_{0.99125}O_3$ ceramic	35	5	1	Solid-state reaction	65	1.85	65	[35]
$Pb_{0.858}Ba_{0.1}La_{0.02}Y_{0.008}Zr_{0.65}Sn_{0.3}Ti_{0.05}$ ceramic	~45	~22	~16	Spark plasma sintering	~28	6.4	62.4	[13]
$0.76NaNbO_3$-$0.24(Bi_{0.5}Na_{0.5})TiO_3$ ceramic	~60	–	–	Solid-state process	680	12.2	69	[43]
$Pb_{0.97}La_{0.02}(Zr_{0.5}Sn_{0.45}Ti_{0.05})O_3$ ceramic	35	~250	~100	Solid-state reaction	400	5.6	67	[12]
Ag_2O-doped $PLZT_{4/90/10}$ ceramic	30	45	18	Solid-phase method	~65	2.22	78.69	[11]
$BiFeO_3$-$BaTiO_3$-$SrTiO_3$ films	69	–	–	PLD	4900	112	80	[2]
$Pb_{(1-3x/2)}La_xZr_{0.85}Ti_{0.15}O_3$ films	60	–	–	Sol-gel	600	38	71	[9]
$Pb_{0.9}La_{0.1}(Zr_{0.52}Ti_{0.48})$ O_3 films	~30	–	–	PLD	1000	12.74	88.44	[4]
$Pb_{0.8}Ba_{0.2}ZrO_3$ (PBZ) films	75	–	–	Sol-gel	2800	40.18	64.1	[15]
$BaTiO_3$/MgO/$BaTiO_3$ films	–	–	–	Electrospinning	4160	15.55	68	[39]
$Ba_{0.7}Ca_{0.3}TiO_3$-$BaZr_{0.2}Ti_{0.8}O_3$ films	37.5	–	–	Magnetron sputtering	4500	52.4	72.3	[14]
$BaZr_{0.35}Ti_{0.65}O_3$ films	–	–	–	RF sputtering	6600	78.7	80.5	[18]
$Pb_{0.96}La_{0.04}Zr_{0.98}Ti_{0.02}O_3$ films	~105	–	–	Sol-gel	4300	61	33	[7]
$Ba(Zr_{0.15}Ti_{0.85})O_3$/$Ba(Zr_{0.35}Ti_{0.65})O_3$ films	40	–	–	Magnetron sputtering	6000	83.9	78.4	[37]
PZO films	30	–	–	PLD	1600	22.4	60.1	[36]
La-modified $PbZrO_3$ films	60	–	–	Sol-gel	600	14.9	–	[20]
6% La-doped $PbZrO_3$ films	45	~520	~310	Sol-gel	1000	~15.2	76	[6]
Sr-doped $PbZrO_3$ films	40	500	300	Sol-gel	900	14.5		[33]
Eu-doped PZO films	~55	–	–	Sol-gel	900	18.8	–	[19]
$Ba_{0.7}Ca_{0.3}TiO_3$/$BaZr_{0.2}Ti_{0.8}O_3$ films	~35	–	–	Solid-state reaction	2860	25.1	63.6[a]	[38]
$(Pb_{0.97}La_{0.02})ZrO_3$ films	103.7	620	340	Sol-gel	800	34.87	59.23	This work
$(Pb_{0.97}La_{0.02})ZrO_3$ films	103.5	620	340	Sol-gel	800	27.98	56.91[a]	This work

a) Data were obtained at the temperature of 200°C.

acetic acid. After the precursor solution was aged for 24 h, PLZO thin films were deposited onto $LaNiO_3$(LNO)/SiO_2/Si substrates. Each layer was deposited, heat-treated at 350°C for 10 min, and annealed at 600°C for 10 min. These steps were repeated until the desired thickness (five layers) was obtained. The films were then crystallized during a 30-min annealing process. To obtain the (110) plane as the preferred orientation, LNO layers with excellent conductivity were heat-treated (400–500°C) and annealed (700°C) by chemical solution deposition [21–25]. The orientations of the thin films were guided by the LNO buffer layers obtained by chemical solution deposition, which were in consistent with those of PBZ, PLZT, and PLZST [9,12,15].

Characterization

The crystalline structure of the thin films was analyzed by using X-ray diffraction (XRD, DX-2700X, China) with Cu Kα radiation at a scanning rate of of 3° min^{-1}. The topography and cross-sectional micrographs of the thin films were obtained by an atomic force microscope (AFM, MFP-3D, Oxford Instrument, UK) and an field emission scanning electron microscope (SEM, SUPPA-55, Zeiss, Germany). For electrical property measurements, platinum electrodes with diameters of 200 μm were generated by direct-current (DC) magnetron sputtering to form a capacity structure. The temperature dependence of the hysteresis loops was characterized by a radiant precision workstation measurement system (TF Analyzer 2000E, aixACCT Systems, Germany) and Lakeshore system from 20 to 210°C with a 30°C interval [21,22].

RESULTS AND DISCUSSION

Structural characterization

Fig. 1 shows the crystal structure and microstructure of the PLZO thin films. A pure perovskite structure is observed, and there is no impurity according to the XRD pattern shown in Fig. 1a. The films have a sharper (110) preferred orientation, which is induced by the orientation of the seeding-layer LNO (110) (as shown between the red lines). The (100) or (110) preferred orientation of the LNO layers can be controlled by the fabrication process [26]. Fig. 1b shows the film morphology of the cross section. The crystallization and layers are clearly discernible, indicating that the microstructure of the PLZO thin films is dense and uniform. The thicknesses of the LNO and PLZO films are approximately 100 and 500 nm, respectively. The high quality of the PLZO films is induced by the LNO seed layers' smooth surfaces, as ob-

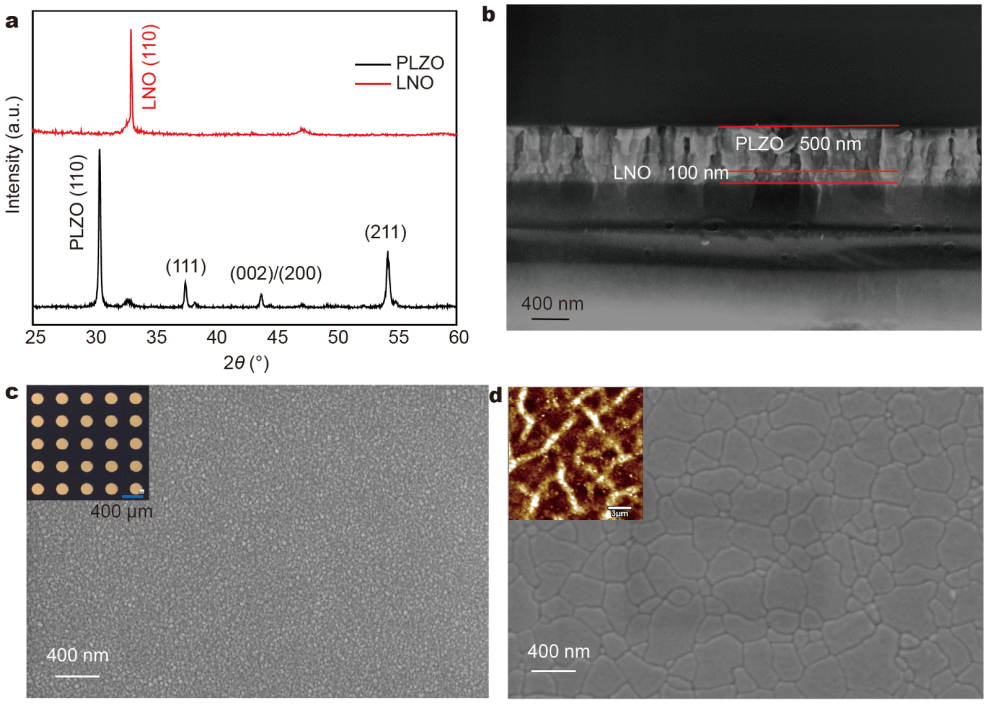

Figure 1 (a) XRD pattern (the red line refers to LNO layers, and the black line refers to PLZO thin films). (b) Cross section of PLZO thin films. (c, d) Top view SEM results of the LNO and PLZO films. Insets in (c, d) show the electrode-size topography and topography of thin films measured by optical microscope and AFM, respectively.

served in Fig. 1c, d. As shown in the inset in Fig. 1d, the films reach a desirable roughness of approximately 1.801 nm. The PLZO thin films present a smooth and uniform crystalline surface, a feature that plays a critical role in the efficiency of energy storage devices.

Hysteresis loops of the PLZO thin films

The thin films exhibit double polarization-voltage (*P*-*E*) loops as shown in Fig. 2a, which is in accordance with previous studies on A-site modification in PZT systems [27,28]. Dipoles are present with antiparallel order to minimize the Gibbs free energy in the initial states, and a relatively small P_r (~7 μC cm^{-2}), which is a typical feature of AFE materials, is noted. The small P_r value may be attributed to the presence of an interface layer between the film and the electrode, which is non-FE with a low dielectric constant and integrated charges during the polarization switching process [10,25]. According to the theory of soft mode, the phase transition process of the AFE materials may be realized by the cancellation of long-range coulombic forces by short-range interactions, as phase transition is based on the balance of competing long-range and short-range forces. Therefore, short-range interactions were the restorative forces in AFE transformation, whereas long-range interactions were the restorative forces in FE transitions. The short-range and long-range interactions between adjacent cations and anions were influenced by an external field; thus, the external electric fields gave a strengthening effect on the long-range coulombic forces and induced the formation of an FE phase. Under external disturbance, domain walls moved, leading to dipole reorientation. The switching current experienced a sharp position corresponding to its phase transition electric field, as shown in Fig. 2a [10]. The corresponding phase transition electric field was obtained by the derivation of the polarization. The phase transition fields can be clearly observed (E_{AF} =620 kV cm^{-1}, E_{FE}=340 kV cm^{-1}) in Fig. 2b, combined with an abrupt current in Fig. 2a. No hysteresis loops are observed when the electric fields are smaller than 600 kV cm^{-1}, as shown in Fig. 2c. According to the Ginzburg-Landau-Devonshire (GLD) phenomenology theory, the energy for the dipole dynamic has a threshold value; very few dipoles can rotate after application of a relatively small field, indicating that La-doped $PbZrO_3$ thin films require a much higher electric field to complete

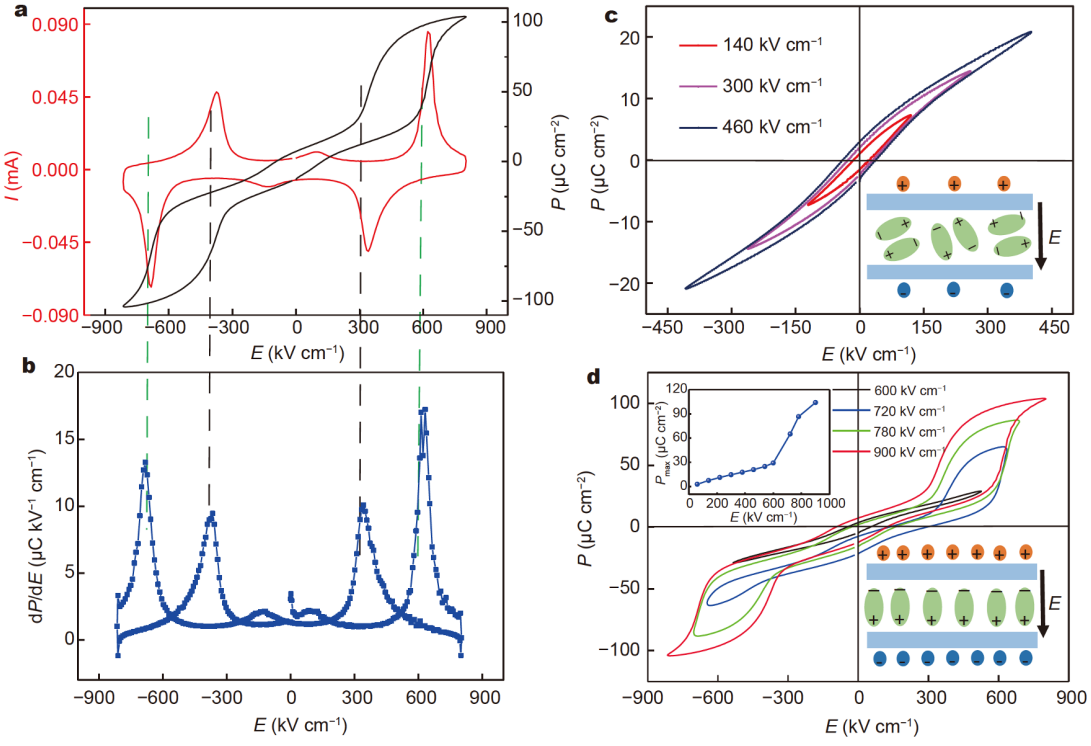

Figure 2 (a) Electrical properties of the thin films under an external electric field. (b) Derivation of the polarization under measurement of (a). Local hysteresis loops of PLZO films under different strengths of electric field, referring to relatively low (c) and high (d) strengths. The inset in (d) shows the electric field dependence of the polarization.

the phase transition process. Under an electric field of 720 kV cm^{-1}, multiple dipoles were reoriented along the electric field direction, and well-developed double hysteresis loops were observed. Thus, phase transition occured with sharp changes in the polarization, as shown in Fig. 2d. The doping with La element decreased the value of *c*/*a* ratio of the unit cell, and the resultant crystal structure of the films approached unity and became pseudo-cubic. Moreover, the unit cell became more asymmetric [6,10], causing a P_{max} of approximately 103.7 μC cm^{-2}. This can be explained by the fact that the La was doped into the A-site to generate Pb vacancies at lower concentrations (2%) than those used in other studies. Because the valence of La ions is higher than that of Pb ions, more Pb vacancies were generated in the films to maintain electrical neutrality. The movement of domain walls was also easier under the same electric field, further promoting polarization reorientation [10]. The inset in Fig. 2d refers to the electric field dependence of P_{max}, more dipole reorientation occurred toward the specific direction under the proper electric fields. Thus, the polarization value of the films increased dramatically upon combining larger electric fields with the phase transition process, which is in consistent with previous studies [10,20].

Energy storage performance of the thin films and temperature stability studies

The temperature dependence of the *P*-*E* loops was studied in the range of 30–210°C, as shown in Fig. 3. The polarization of the AFE films showed a slight increase and then decrease, with increasing temperature as shown in Fig. 3a. This can be explained from the fact that La^{3+} doping is a controversial issue divided by destroying and stabilizing the long-range order of the dipoles, which stabilizes the AFE or FE phase [10]. In these fabricated films, the low concentration doping of La^{3+} destroyed the long-range order of the dipoles, thus stabilizing the AFE phase. Therefore, more dipoles were reoriented with an external bias and increasing temperature, and phase transition was achieved, causing a slight increase in polarization. However, at high temperatures, FE states were formed, decreasing polarization owing to lattice symmetry, which is in consistent with the previous report [22]. The stability of the thin films can be characterized by the tolerance factor (*t*), which is given as follows:

$$t = \frac{r_A + r_O}{\sqrt{2}(r_B + r_O)}, \quad (1)$$

where r_A, r_B, and r_O are the ionic radii of the A-site and B-site cations and oxygen anion, respectively.

$$r_A = 0.97 r_{Pb^{2+}} + 0.02 r_{La^{3+}}, \quad (2)$$

$$r_B = r_{Zr^{4+}}. \quad (3)$$

The ionic radii (*r*) of Pb^{2+}, La^{3+}, Zr^{4+}, and O^{2-} are 0.149, 0.136, 0.072, and 0.061 nm, respectively. The value of *t* is 0.9679, according to Equations (1–3). The decrease in *t* can be ascribed to the doping effect of La^{3+}, whose ionic radius is smaller. The doping of an ion with a smaller ion enhances the stability of the AFE phase states [20,29,30]. Therefore, a higher electric field E_{AF} is required to transform the AFE phase into an FE phase, which is beneficial for the enhancement of energy storage density [9]. The PLZO films could be transformed into FE states under an external factor, and the induction of the phase transformation caused by temperature was synergistic

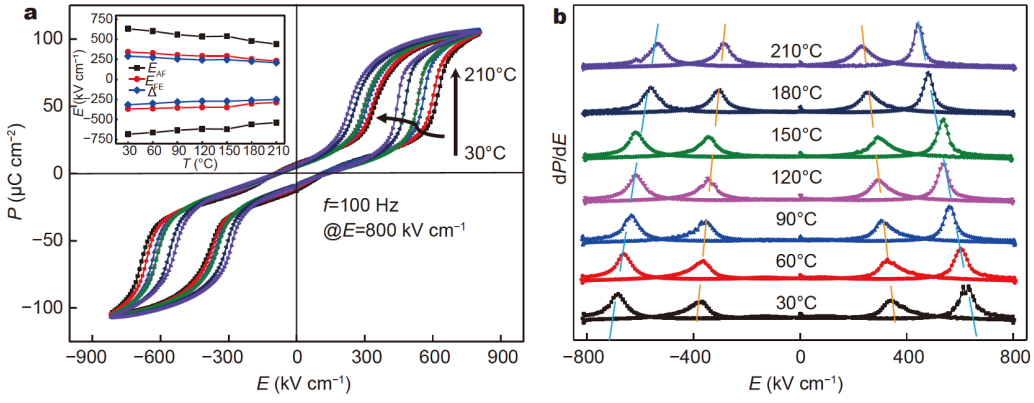

Figure 3 Temperature dependence of the electrical property of the PLZO films. (a) Effect of temperature on the electrical properties of thin films. (b) Derivation of the polarization by the electric field under different temperatures. The inset in Fig. 3a shows the critical phase transition voltage (including positive, negative, and the difference between them).

with the induction of the phase change by the external field, as observed in Fig. 3a [22]. The processes of the domain nucleation and dipole reorientation of materials were affected by the external environment, which induced a variation in energy storage performance. As the temperature increased, the phase transformation electric fields decreased owing to the barrier reduction required for domain inversion [7,10]. The difference between the electric fields of E_{AF}–E_{FE} also gradually decreased. The decrease in the switching field implies that different free energies between the two phases were shrinking. Therefore, for the PLZO thin films, the AFE phase became unstable as the temperature increased, as indicated by the *P-E* loops that gradually become slimmer (as observed in the inset of Fig. 3a)

Thermal stability is an important factor affecting the energy storage properties. Fig. 4 shows the temperature dependence of the energy storage performance under external electric fields. The recoverable energy storage density (W_{rec}) is shown in the green region of the inset of Fig. 4a, and it can be calculated by the numerical integration of the hysteresis loops as follows [31,32]:

$$w_{rec} = \int_{P_r}^{P_{max}} E\mathrm{d}P, \tag{4}$$

$$w_{total} = \int_{0}^{P_{max}} E\mathrm{d}P. \tag{5}$$

Considering the device applications, high energy efficiency (η) combined with a low loss density (J_{loss}) is preferable, and the efficiency η is expressed as follows:

$$\eta = \frac{w_{rec}}{w_{total}} \times 100\%. \tag{6}$$

Films with larger polarization are preferable for practical applications. The result shows that P_{max} and P_r are approximately 103.7 and 7.28 μC cm^{-2} at room temperature, respectively. As shown in Fig. 4a, the polarization states were obviously affected by temperature. The P_{max} increases with temperature at first and then decreased slightly at higher temperatures. It is believed that the stability of AFE phase is enhanced by combining the doping element with smaller ions. Since the AFE phase

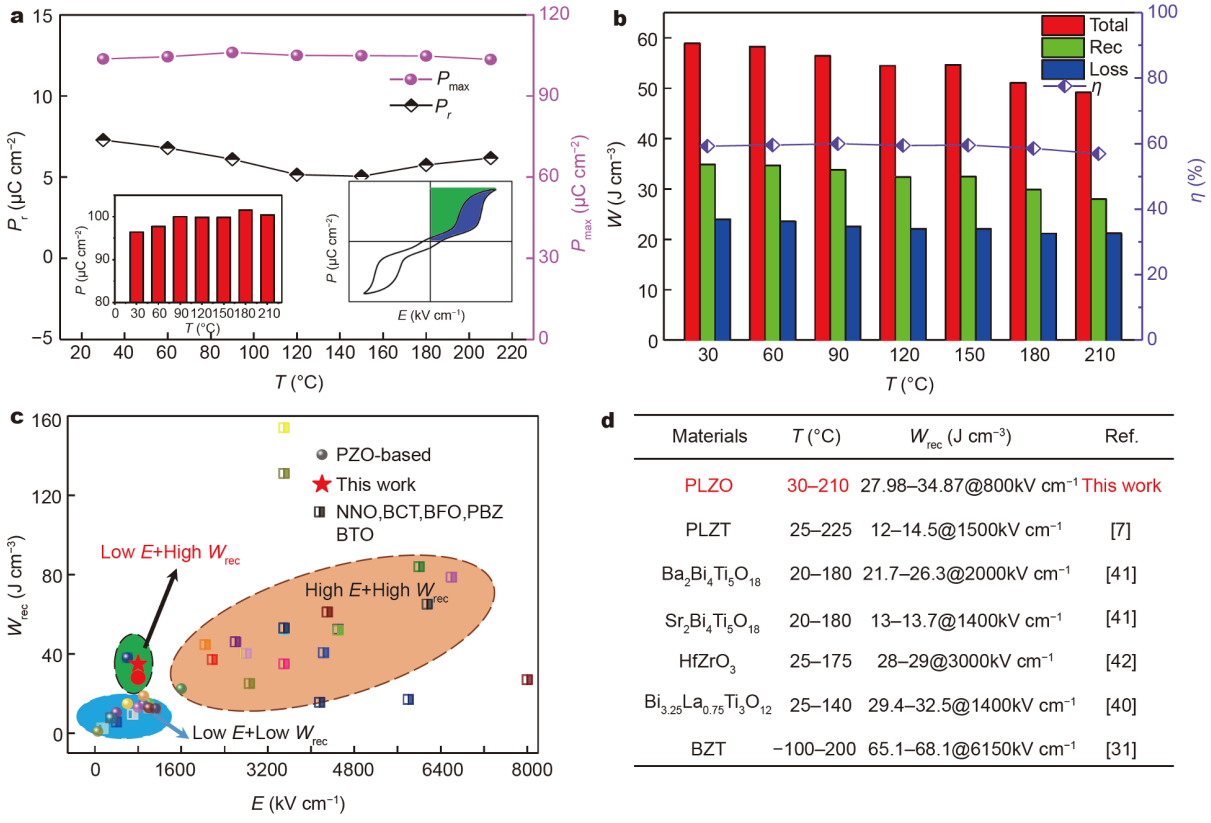

d

Materials	T (°C)	W_{rec} (J cm^{-3})	Ref.
PLZO	30–210	27.98–34.87@800kV cm^{-1}	This work
PLZT	25–225	12–14.5@1500kV cm^{-1}	[7]
$Ba_2Bi_4Ti_5O_{18}$	20–180	21.7–26.3@2000kV cm^{-1}	[41]
$Sr_2Bi_4Ti_5O_{18}$	20–180	13–13.7@1400kV cm^{-1}	[41]
$HfZrO_3$	25–175	28–29@3000kV cm^{-1}	[42]
$Bi_{3.25}La_{0.75}Ti_3O_{12}$	25–140	29.4–32.5@1400kV cm^{-1}	[40]
BZT	−100–200	65.1–68.1@6150kV cm^{-1}	[31]

Figure 4 Temperature dependence of the electrical characteristics of the PLZO films. (a) Relationship between P_{max} and P_r corresponding to temperature. The insets in (a) show the difference of P_{max}–P_r and the schematic diagram of energy storage, respectively. (b) Temperature dependence of the energy storage performance of the thin films within a range of 30–210°C. (c, d) Comparison of the energy storage performances for selected materials.

became unstable with increase in temperature, phase transition occurred, combined with an increase in polarization [10,28]. The phase transition process from AFE to FE state can easily occur at higher temperatures; the structure of the unit cells also became more symmetrical as the temperature increased, causing a slight decrease in polarization. With regard to P_r, the extremely small dynamic might be induced by the pinning effect of domain. In addition, a large difference between P_{max} and P_r is apparent as shown in the inset of Fig. 4a, which is highly beneficial to the enhancement of energy storage performance.

As can be seen in Fig. 4b, the W_{rec} under rather low electric field was approximately 34.87 J cm^{-3} with storage efficiency of 59.23%, compared with that of single-composition films [20], Sr-doped $PbZrO_3$ (14.5 J cm^{-3}) [33], and La-doped $PbZrO_3$ films (15.2 J cm^{-3}, 14.9 J cm^{-3}) [6,20], as shown in Fig. 4 and Table 1. Fig. 4b illustrates that the energy performance of the total/recovery/loss also experienced a slight decrease as temperatures increased from 30 to 210°C. The recovery energy of the thin films decreased from 34.87 to 27.98 J cm^{-3}, and the efficiency showed a slight decrease from 59.23% to 56.91% (energy storage efficiency was lower than in other studies [6,7,9,11–14,18,20,33,34,42], which might be due to the high incidence of domain reversion during the phase transformation process; further improvement is needed to the enhancement of efficiency). The performance of the PLZO films under rather low electric fields demonstrated excellent storage properties and temperature stability compared with other materials, as shown in Fig. 4c, d. The slight decrease in efficiency can be attributed to the fact that dipoles are reoriented as temperature increases, causing the lattice to become more symmetrical, which leads to a decrease in polarization. The pinning effect of domain causes a slight increase in P_r in the range of 140–220°C [10]. Moreover, the leakage current increases with temperature, which may lead to an additional loss [7]. Due to the high temperature stability under low electric fields, these films offer great potential

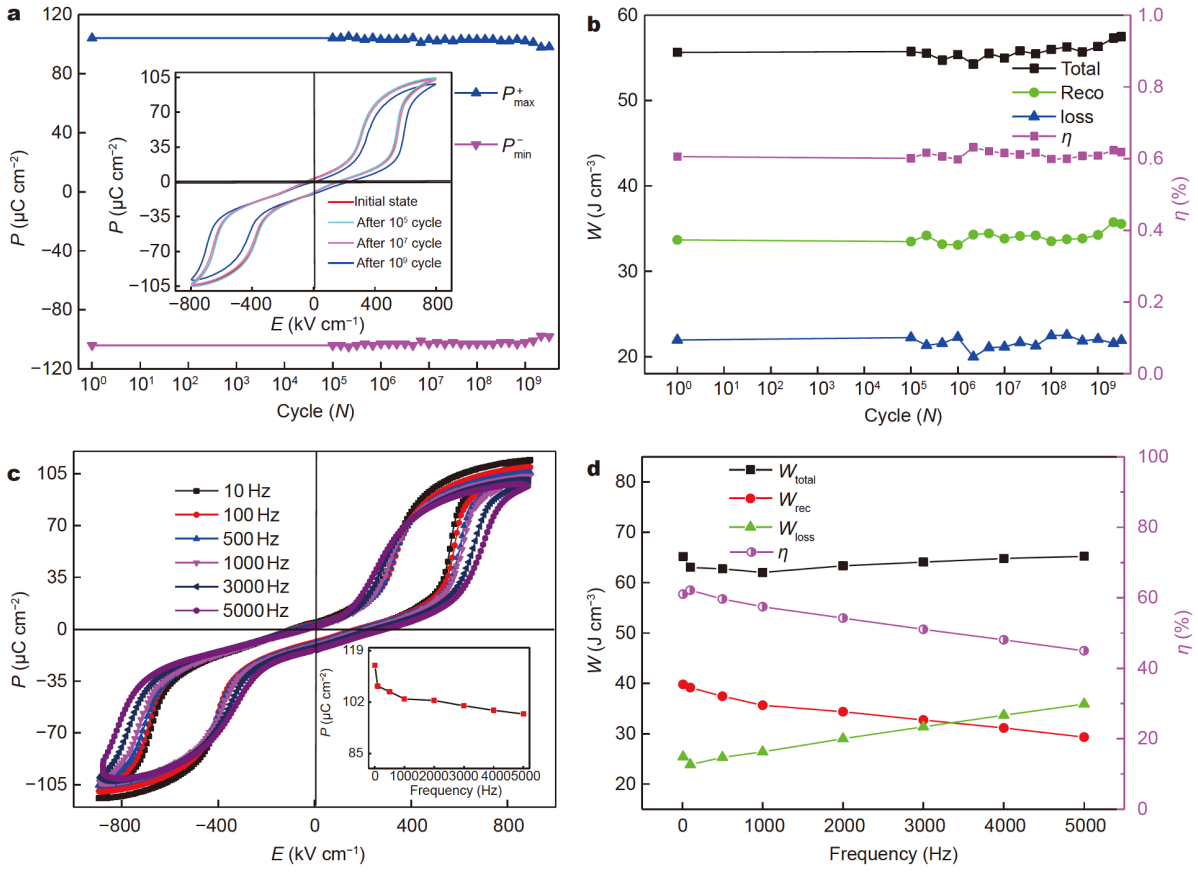

Figure 5 (a) Fatigue performance of the thin films. The inset shows *P-E* hysteresis loops before and after 10^9 cycles of the capacitors. (b) Energy storage properties after cycling, showing a nearly constant W_{rec} and efficiency. (c) *P-E* hysteresis loops under various frequency activations. The inset shows the frequency dependence of electric displacement. (d) Energy storage densities and efficiencies under different test frequencies.

for device applications in low-consumption systems under harsh conditions.

Long-term working stability is also a critical factor for device applications. Fig. 5 shows the fatigue properties and energy storage properties of the PLZO thin films, represented by adding a triangular wave to the capacity structure with frequency of 100 kHz and electric field bias of 800 kV cm^{-1}. The P_{max} of the thin films decreased by 5.77%, from 104 to 97.7 μC cm^{-2} after 3.18×10^9 cycles, with almost no deterioration in the measurement range, as shown in the inset of Fig. 5a. It can be clearly seen in Fig. 5b that the films exhibited little degradation in either W_{rec} or η after 3×10^9 cycles. The LNO layers provide strong lattice match as well as the reduction of oxygen vacancies [16], which improve the fatigue endurance of the thin films [7,10].

Fig. 5c, d additionally show the frequency dependence of electrical properties. As shown in Fig. 5c, the quantity of dipoles rotation decreases as the frequency increases, resulting in decrease in polarization value. The W_{rec} in Fig. 5d appears almost constant, and varies from 39.78 to 29.32 J cm^{-3} as frequencies increase from 10 to 5000 Hz, which is superior to the results in literature [44]. When the operating frequency increased from 10 to 3000 Hz, the efficiency of recovery remained above 51%. The maximum value of W_{rec} was 39.78 J cm^{-3} at 10 Hz in the La-doped AFE films, indicating numerous prospects for applications in high-frequency pulsed devices and systems.

The excellent performance of thin films can be attributed to their high degree of compaction and the doping effect. With regard to the production process, an LNO buffer layer provided better guidance for the films' orientation, and the oxide electrode enabled better polarization endurance (PE) than the traditional Pt/Ti electrode, leading to excellent fatigue properties [6,9,10,26,40]. The enhancement of PE may be due to the decrease in oxygen vacancy density and the suppressed mobility resulting from ionic doping [16]. With regard to the excellent energy storage performance, the crystal structure of the films approached uniformity and became pseudo-cubic by the doping element, resulting in a more asymmetrical unit cell structure and subsequent enhancement of the polarization property [6,10]. The stability of the AFE phase would be improved by smaller ionic doping compared with the A-site (Pb) [10,20,28,30,33]. Once the stability of anti-ferroelectricity improved, the potential well corresponding to the phase transition became deeper, revealing that a larger electric field is required for crossing the energy barrier. According to the relation of $W = \int E\mathrm{d}P$ and the diagram of energy storage (inset in Fig. 4a), an enhancement of P or the phase transition threshold value from the AFE phase to the FE phase leads to the enhancement of W values. Moreover, the temperature stability of the energy storage is comparable to that in reported studies [7,16,31,40–42], which represents a tremendous advantage of pulsed power devices in strenuous conditions.

CONCLUSIONS

PLZO thin films exhibiting high energy storage density and excellent temperature stability under low electric fields were fabricated using the sol-gel method. Subsequently, the temperature dependence of the electric properties of the thin films was systematically investigated. The local hysteresis loops revealed the reorientation of dipoles under external electric fields. A giant polarization of approximately 103.7 μC cm^{-2} was obtained owing to the vacancies of Pb at a medium field of ~800 kV cm^{-1}. The recovery energy storage density of 34.87 J cm^{-3} with an efficiency of 59.23% was observed under ~800 kV cm^{-1}, which is much lower than the electric fields used in other studies. However, further efforts are required for enhancing the efficiency. The thin films exhibited little deterioration at high temperatures (27.98 J cm^{-3} at 210°C) and during fatigue tests (up to ~10^9 cycle), and the recoverable energy storage density varied between 39.78 and 29.32 J cm^{-3} combined with an efficiency of 61.03%–44.95% (under electric fields of 900 kV cm^{-1} and test frequencies from 10 to 5000 Hz), which reveals that the developed materials would be suitable candidates for low-consumption pulsed energy storage systems and applications in harsh environment.

Received 6 February 2020; accepted 6 May 2020; published online 11 August 2020

1 Tang Z. Non-noble metal anode based dual-ion batteries: Promising high-energy and low-cost energy storage devices. Sci China Mater, 2017, 60: 368–370
2 Pan H, Li F, Liu Y, *et al.* Ultrahigh-energy density lead-free dielectric films *via* polymorphic nanodomain design. Science, 2019, 365: 578–582
3 Wang X, Lu X, Liu B, *et al.* Flexible energy-storage devices: Design consideration and recent progress. Adv Mater, 2014, 26: 4763–4782
4 Nguyen CTQ, Nguyen MD, Vu HT, *et al.* High energy storage responses in all-oxide epitaxial relaxor ferroelectric thin films with the coexistence of relaxor and antiferroelectric-like behaviors. Thin Solid Films, 2017, 636: 188–192
5 Wu Y, Cao C. The way to improve the energy density of supercapacitors: Progress and perspective. Sci China Mater, 2018, 61: 1517–1526

6 Lee HJ, Won SS, Cho KH, *et al.* Flexible high energy density capacitors using La-doped $PbZrO_3$ anti-ferroelectric thin films. Appl Phys Lett, 2018, 112: 092901
7 Hu Z, Ma B, Koritala RE, *et al.* Temperature-dependent energy storage properties of antiferroelectric $Pb_{0.96}La_{0.04}Zr_{0.98}Ti_{0.02}O_3$ thin films. Appl Phys Lett, 2014, 104: 263902
8 Adak B, Chinya I, Sen S. Enhanced dielectric and energy storage performance of surface treated gallium ferrite/polyvinylidene fluoride nanocomposites. RSC Adv, 2016, 6: 105137
9 Zhao Y, Hao X, Zhang Q. Energy-storage properties and electrocaloric effect of $Pb_{(1-3x/2)}La_xZr_{0.85}Ti_{0.15}O_3$ antiferroelectric thick films. ACS Appl Mater Interfaces, 2014, 6: 11633–11639
10 Hao X, Zhai J, Kong LB, *et al.* A comprehensive review on the progress of lead zirconate-based antiferroelectric materials. Prog Mater Sci, 2014, 63: 1–57
11 Zhao T, Zhu Q, Xu R, *et al.* Effects of Ag_2O doping on dielectric properties of $(Pb_{0.96}La_{0.04})(Zr_{0.9}Ti_{0.1})_{0.99}O_3$ antiferroelectric ceramics. Ceram Int, 2019, 45: 1887–1892
12 Chen S, Wang X, Yang T, *et al.* Composition-dependent dielectric properties and energy storage performance of (Pb,La)(Zr,Sn,Ti)O_3 antiferroelectric ceramics. J Electroceram, 2014, 32: 307–310
13 Zhang L, Jiang S, Fan B, *et al.* Enhanced energy storage performance in $(Pb_{0.858}Ba_{0.1}La_{0.02}Y_{0.008})(Zr_{0.65}Sn_{0.3}Ti_{0.05})O_3$–$(Pb_{0.97}La_{0.02})$-$(Zr_{0.9}Sn_{0.05}Ti_{0.05})O_3$ anti-ferroelectric composite ceramics by spark plasma sintering. J Alloys Compd, 2015, 622: 162–165
14 Sun Z, Ma C, Liu M, *et al.* Ultrahigh energy storage performance of lead-free oxide multilayer film capacitors *via* interface engineering. Adv Mater, 2017, 29: 1604427
15 Peng B, Zhang Q, Li X, *et al.* Large energy storage density and high thermal stability in a highly textured (111)-oriented $Pb_{0.8}Ba_{0.2}ZrO_3$ relaxor thin film with the coexistence of antiferroelectric and ferroelectric phases. ACS Appl Mater Interfaces, 2015, 7: 13512–13517
16 Ye M, Sun Q, Chen XQ, *et al.* Effect of Eu doping on the electrical properties and energy storage performance of $PbZrO_3$ antiferroelectric thin films. J Am Ceram Soc, 2011, 94: 3234–3236
17 Ahn CW, Amarsanaa G, Won SS, *et al.* Antiferroelectric thin-film capacitors with high energy-storage densities, low energy losses, and fast discharge times. ACS Appl Mater Interfaces, 2015, 7: 26381–26386
18 Wang Z, Zhao K, Guo X, *et al.* Crystallization, phase evolution and ferroelectric properties of sol-gel-synthesized $Ba(Ti_{0.8}Zr_{0.2})O_{3-x}$-$(Ba_{0.7}Ca_{0.3})TiO_3$ thin films. J Mater Chem C, 2013, 1: 522–530
19 Liang Z, Liu M, Ma C, *et al.* High-performance $BaZr_{0.35}Ti_{0.65}O_3$ thin film capacitors with ultrahigh energy storage density and excellent thermal stability. J Mater Chem A, 2018, 6: 12291–12297
20 Parui J, Krupanidhi SB. Enhancement of charge and energy storage in sol-gel derived pure and La-modified $PbZrO_3$ thin films. Appl Phys Lett, 2008, 92: 192901
21 Peng B, Zhang Q, Lyu Y, *et al.* Thermal strain induced large electrocaloric effect of relaxor thin film on $LaNiO_3$/Pt composite electrode with the coexistence of nanoscale antiferroelectric and ferroelectric phases in a broad temperature range. Nano Energy, 2018, 47: 285–293
22 Geng W, Liu Y, Meng X, *et al.* Giant negative electrocaloric effect in antiferroelectric La-doped $Pb(ZrTi)O_3$ thin films near room temperature. Adv Mater, 2015, 27: 3165–3169
23 Chen X, Qiao X, Zhang L, *et al.* Temperature dependence of ferroelectricity and domain switching behavior in $Pb(Zr_{0.3}Ti_{0.7})O_3$ ferroelectric thin films. Ceram Int, 2019, 45: 18030–18036
24 Zhang Q, Geng W, Zhang J, *et al.* Effect of electrode interfaces on peak-drift switching current of PZT thin films. Ceram Int, 2019, 45: 3159–3165
25 Nguyen MD, Rijnders G. Thin films of relaxor ferroelectric/antiferroelectric heterolayered structure for energy storage. Thin Solid Films, 2018, 659: 89–93
26 Wang GS, Zhao Q, Meng XJ, *et al.* Preparation of highly (100)-oriented $LaNiO_3$ nanocrystalline films by metalorganic chemical liquid deposition. J Cryst Growth, 2005, 277: 450–456
27 Li B, Liu Q, Tang X, *et al.* High energy storage density and impedance response of PLZT2/95/5 antiferroelectric ceramics. Materials, 2017, 10: 143
28 Parui J, Krupanidhi SB. Effect of La modification on antiferroelectricity and dielectric phase transition in sol-gel grown thin films. Solid State Commun, 2010, 150: 1755–1759
29 Qiao P, Zhang Y, Chen X, *et al.* Effect of Mn-doping on dielectric and energy storage properties of $(Pb_{0.91}La_{0.06})(Zr_{0.96}Ti_{0.04})O_3$ antiferroelectric ceramics. J Alloys Compd, 2019, 780: 581–587
30 Liu J, Geng W, Chou X, *et al.* Electric-field-induced antiferroelectric to ferroelectric and ferroelectric to paraelectric phase transition at various temperatures in (Pb, La)(Zr, Ti)O_3 antiferroelectric thick films. J Sol-Gel Sci Technol, 2012, 62: 414–418
31 Liang Z, Ma C, Shen L, *et al.* Flexible lead-free oxide film capacitors with ultrahigh energy storage performances in extremely wide operating temperature. Nano Energy, 2019, 57: 519–527
32 Liu Z, Chen X, Peng W, *et al.* Temperature-dependent stability of energy storage properties of $Pb_{0.97}La_{0.02}(Zr_{0.58}Sn_{0.335}Ti_{0.085})O_3$ antiferroelectric ceramics for pulse power capacitors. Appl Phys Lett, 2015, 106: 262901
33 Hao X, Zhai J, Yao X. Improved energy storage performance and fatigue endurance of Sr-doped $PbZrO_3$ antiferroelectric thin films. J Am Ceram Soc, 2009, 92: 1133–1135
34 Zhao L, Liu Q, Zhang S, *et al.* Lead-free $AgNbO_3$ anti-ferroelectric ceramics with an enhanced energy storage performance using MnO_2 modification. J Mater Chem C, 2016, 4: 8380–8384
35 Ciuchi IV, Mitoseriu L, Galassi C, *et al.* Antiferroelectric to ferroelectric crossover and energy storage properties of $(Pb_{1-x}La_x)$-$(Zr_{0.90}Ti_{0.10})_{1-x/4}O_3$ ($0.02 \le x \le 0.04$) ceramics. J Am Ceram Soc, 2016, 99: 2382–2387
36 Nguyen MD, Rijnders G. Electric field-induced phase transition and energy storage performance of highly-textured $PbZrO_3$ antiferroelectric films with a deposition temperature dependence. J Eur Ceram Soc, 2018, 38: 4953–4961
37 Fan Q, Liu M, Ma C, *et al.* Significantly enhanced energy storage density with superior thermal stability by optimizing $Ba(Zr_{0.15}$-$Ti_{0.85})O_3$/$Ba(Zr_{0.35}Ti_{0.65})O_3$ multilayer structure. Nano Energy, 2018, 51: 539–545
38 Sun Z, Wang L, Liu M, *et al.* Interface thickness optimization of lead-free oxide multilayer capacitors for high-performance energy storage. J Mater Chem A, 2018, 6: 1858–1864
39 Li Z, Liu F, Li H, *et al.* Largely enhanced energy storage performance of sandwich-structured polymer nanocomposites with synergistic inorganic nanowires. Ceram Int, 2019, 45: 8216–8221
40 Yang BB, Guo MY, Song DP, *et al.* $Bi_{3.25}La_{0.75}Ti_3O_{12}$ thin film capacitors for energy storage applications. Appl Phys Lett, 2017, 111: 183903
41 Yang B, Guo M, Tang X, *et al.* Lead-free $A_2Bi_4Ti_5O_{18}$ thin film capacitors (A=Ba and Sr) with large energy storage density, high efficiency, and excellent thermal stability. J Mater Chem C, 2019, 7: 1888–1895

42 Park MH, Kim HJ, Kim YJ, *et al.* Thin $Hf_xZr_{1-x}O_2$ films: A new lead-free system for electrostatic supercapacitors with large energy storage density and robust Thermal stability. Adv Energy Mater, 2014, 4: 1400610
43 Qi H, Zuo R, Xie A, *et al.* Ultrahigh energy-storage density in $NaNbO_3$-based lead-free relaxor antiferroelectric ceramics with nanoscale domains. Adv Funct Mater, 2019, 29: 1903877
44 Chen MJ, Ning XK, Wang SF, *et al.* Significant enhancement of energy storage density and polarization in self-assembled $PbZrO_3$: NiO nano-columnar composite films. Nanoscale, 2019, 11: 1914–1920

Acknowledgements This work was supported by the National Key R&D Program of China (2018YFE0115500), the National Natural Science Foundation of China (61704159 and 51975541), Shanxi Province Science Foundation for Youths (201701D221125 and 201801D221199), Program for the Young Academic Leaders of the North University of China (QX201807), the Research Project Supported By Shanxi Scholarship Council of China (2019-066), and Shanxi "1331 Project" Key Subject Construction (1331 KSC).

Author contributions Geng W and Qiao X designed the devices and experiments; Qiao X, Chen X, Zhang L, Yang Y and Zheng D performed the experiments; Qiao X, Zhang L, He J, Cui M, and Hou X analyzed the data; Qiao X wrote the paper with support from Geng W, Zeng K and Chou X. All authors contributed to the general discussion.

Conflict of interest The authors declare that they have no conflict of interest.

Xiaojun Qiao obtained his BSc degree in 2013 from Shenyang Ligong University. Currently, he is a PhD student at Science and Technology on Electronic Test and Measurement Laboratory in North University of China (NUC). His main research topics are energy storage system toward pulse power applications.

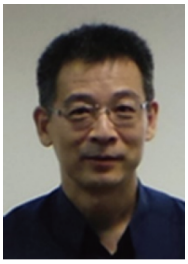

Kaiyang Zeng is associate professor at the Department of Mechanical Engineering, National University of Singapore. He got his PhD degree in materials science from the Royal Institute of Technology (KTH), Sweden. His main research areas include the use of scanning probe microscopy-based techniques to study multifield coupling phenomena in advanced materials, such as high-performance piezo/ferroelectric materials, biomaterials, supramolecular materials, oxide materials, and energy storage materials.

Xiujian Chou works at the School of Instrument and Electronics of the NUC. He received his PhD degree in material physics and chemistry at Tongji University in 2008. Currently, he is engaged in research on intelligent micro/nano devices and micro system.

低电场下耐疲劳La掺杂$PbZrO_3$薄膜的储能特性及温度稳定性研究

乔骁骏[1], 耿文平[1], 陈茜[1], 张乐[1], 郑冬宛[1], 张辽原[1], 何剑[1], 侯晓娟[1], 杨云[1], 崔敏[1], 曾开阳[2*], 丑修建[1*]

摘要 为了满足恶劣环境下低功耗脉冲功率器件的需求, 具有超高储能密度和温度稳定性的静电储能电容器受到广泛关注. 本研究在较低的电场激励作用和极宽的温度范围内获得了高储能性能的反铁电薄膜. 采用溶胶-凝胶法制备了La掺杂的$PbZrO_3$薄膜, 在~800 kV cm^{-1}电场下, 室温下可释放储能密度34.87 J cm^{-3}, 储能效率为59.23%. 此外, 该储能特性具有优良的温度稳定性(210°C下储能密度为27.98 J cm^{-3})、 抗疲劳特性(3×10^9次循环后无明显疲劳)以及频率稳定性(储能密度: 39.78–29.32 J cm^{-3}; 储能效率: 61.03%–44.95%) (测试频率10–5000 Hz, 电场为~900 kV cm^{-1}). 反铁电薄膜储能性能提升主要是由于$LaNiO_3$缓冲层以及掺杂产生铅空位而引起的高极化值(P_{max}约为103.7 μC cm^{-2})和较低的剩余极化(P_r ~7 μC cm^{-2}), 为脉冲功率器件在低功耗系统中的应用奠定了研究基础.

